

BOUNDARY LAYER INDUCED BY A CONICAL VORTEX

by R. FERNANDEZ-FERIA and J. C. ARRESE

(Universidad de Málaga, E.T.S.Ingenieros Industriales, 29013 Málaga, Spain)

[Received 27 May 1998. Revises 14 January, 19 July 1999 and 26 April 2000]

Summary

The structure of the boundary layer induced by a family of inviscid vortices with conical symmetry over a solid plane is analysed. Though the equations governing the problem over an infinite plane may be written in a self-similar form, they have no self-similar solutions connecting the no-slip boundary condition at the plane with the inviscid external vortex. Numerical computations on a finite circular disk of radius R suggest new variables in terms of which the solution tends to an asymptote as the axis is approached. Further, a similarity solution for the finite disk problem is given. This solution provides a relatively simple 'initial' velocity profile to consistently model the effusing core structure in actual vortices of interest.

1. Introduction

The interaction of nearly inviscid vortices with plane and conical walls has been considered by a number of authors owing to its relevance in the description of different flows of technological interest (for example, vortex chambers, vortex separators, combustion chambers) and atmospheric interest (for example, tornadoes, dust whirls, waterspouts). Taylor (1) was the first to analyse the laminar boundary-layer structure induced by a potential vortex on a conical surface coaxial with the vortex in relation to the swirl atomizer problem. In cylindrical polar coordinates (r, θ, z) , used throughout the present work, the velocity field (u, v, w) of the external potential vortex may be written as

$$(u, v, w) = (0, \Gamma/r, 0), \quad (1)$$

where the circulation $2\pi\Gamma$ is constant. Taylor made use of a momentum integral method to solve the laminar boundary-layer equations resulting from the interaction of this vortex with a conical surface. Integral methods were also used later by other investigators in connection with this problem (see, for example, the review by Rott and Lewellen (2)). However, these methods, though appropriate in obtaining several global properties of the boundary layer, fail to describe the details of its structure, which was later shown to have interesting properties. For instance, King and Lewellen (3) looked for similarity solutions to the boundary-layer equations governing the interaction with a plane of a family of inviscid vortices a little more general than (1):

$$(u, v, w) = (0, \Gamma_n/r^n, 0), \quad (2)$$

where n ranges from -1 (solid-body rotation) to 1 (potential vortex). Surprisingly, these authors found that the resulting set of two ordinary differential equations governing the problem does not have a solution for every value of n in the range investigated. In particular, the equations have no solution for the potential vortex case ($n = 1$; see also (2)). Similarity solutions for an infinite plane were found by these authors for values of n in the interval $-1 \leq n \leq 0.1$ (for $n = -1$ the similarity solution is obviously that found earlier by Bödewadt (4)). The interaction of a potential

vortex like (1) with a plane was later investigated by Burggraf *et al.* (5) and Prahlad and Head (6), who integrated numerically the boundary-layer equations over a disk of finite radius. Though the set of ordinary differential equations resulting from the *natural* self-similar variables of the problem (without length scale) was shown to have no solution satisfying the no-slip boundary condition, from the numerical solution to the parabolic boundary-layer equations on a finite disk, Burggraf *et al.* (5) were able to find a different similarity solution with a double layer structure for the finite plane problem (see also Carrier *et al.* (7) for a simpler formulation of this double-layer structure). This work was subsequently generalized by Belcher *et al.* (8) to the more general family of inviscid vortices of the form (2). They found numerically that a self-similar solution to the boundary-layer equations for the infinite plane problem exists when $-1 \leq n \leq 0.1217$. For larger values of n no self-similar solutions exist, but, from the numerical integration of the equations on a finite disk, these authors were again able to find a two-layer self-similar structure for the boundary layer over a finite plane.

Although the family of inviscid vortices (2) covers a wider class of flows than (1), being more in agreement with real high Reynolds number swirling flows, where experimental measurements of the azimuthal velocity in both confined and open flows (vortex chambers, tornadoes, etc.) yield values of n ranging between 0.4 and 1 (see, for example, Ogawa (9) for a review of experimental measurements in very different types of vortices), it shares the same limitation of having no meridional motion; that is, $u = w = 0$. Many vortices of practical interest have a meridional motion as important as the azimuthal one even at the external inviscid level, and it is therefore essential to take it into account in order to study the interaction of real vortices with plane walls. A particular swirling flow with meridional motion extensively studied in the literature is the family of conical vortices with velocity field inversely proportional to the distance from the origin, which in cylindrical polar coordinates may be written as

$$\mathbf{u} = \mathbf{V}(y) \frac{1}{r}, \quad y = r/z, \quad (3)$$

where $\mathbf{V}(y)$ is a vector function whose three components may be obtained from the integration of just two ordinary differential equations (see, for example, Sozou (10)). In fact, this is the only instance of a flow with conical symmetry for which the full Navier–Stokes equations for an incompressible fluid can be written in similarity form. It has often been used as an idealized model for a tornado (for example, Serrin (11), Shtern and Hussain (12), among others), displaying some of its interesting properties. However, it was first shown by Goldshnik (13), and then by Serrin (11) and others, that these solutions are either singular at the axis or cannot satisfy the adherence boundary condition at the wall above a critical value of the Reynolds number—whence the non-existence of self-similar solutions for the boundary layer induced by an inviscid vortex of the form (3). A similar conclusion was drawn recently (14) for the more general family of inviscid conical flows of the form

$$\mathbf{u} = \mathbf{V}(y) r^{m-2}, \quad (4)$$

where $0 < m < 2$, which includes the above mentioned range of values of m for the measured radial dependence of the azimuthal velocity outside the vortex core in several flows of practical interest ($1 \leq m \leq 1.6$, approximately; see (9)). The case $m = 1$ corresponds to (3), for which the full Navier–Stokes equations can be written in similarity form. For $m \neq 1$, the Navier–Stokes equations have no solutions of the form (4), but the Euler equations do. It is shown in (14) that for these inviscid flows the three components of the vector function \mathbf{V} are obtained by the integration of just

one ordinary differential equation. However, this inviscid solution is singular at the axis ($y = 0$) and at the plane ($y \rightarrow \infty$) for $0 < m < 2$ (more precisely, the inviscid flow is singular both at the axis and at any other conical surface that shares the inviscid meridional streamlines with it). The axial regularization through a self-similar viscous core (15) shows that only certain ranges of the swirl parameter L , or ratio of near-axis inviscid azimuthal velocity to axial velocity,

$$L = (v/w)_{y=0}, \quad (5)$$

are allowed. These ranges of permissible values of L depend on m . For $0 < m < 1$ there is a minimum value of L for each m , so that swirlless flows are not possible. For the case $m = 1$ the near-axis boundary layer flow corresponds to the well-known Long's (16) vortex, and it is found that the only allowed value is $L = \sqrt{2}$ (due to the so-called *collapse* phenomenon; see Goldshnik and Shtern (17)), so that meridional motion and swirl are necessarily coupled in this case. For $1 < m < 2$, it is found that for each value of m there exists a maximum value of L above which no solution exists, in qualitative agreement with vortex breakdown of real flows (for m slightly larger than unity, the maximum value of L found in (15) is in quantitative agreement with the critical value of the swirl parameter for vortex breakdown of high Reynolds number swirling flows). On the other hand, independently of the value of m , only *inviscid* flows going upward along the axis can be regularized through a near-axis boundary layer, corresponding to radial motions directed inward along the plane.

The main objective of the present work is to analyse the boundary-layer structure induced by inviscid flows of the form (4) on a plane wall (as a matter of fact, the results given here are also valid for the boundary layer on any conical wall coaxial with the vortex). In particular, we shall consider the range $1 \leq m < 2$, which includes the most interesting cases from a physical point of view ($1 \leq m \leq 1.6$, approximately). It was shown in (14) (see also Appendix B) that no self-similar solutions to the boundary-layer equations over an infinite plane compatible with the boundary condition of zero velocity at the wall exist (although other boundary conditions may be allowed), in spite of the similarity nature of the problem. This is in agreement with the above mentioned known result from the full Navier–Stokes equations for the particular case $m = 1$. Thus, though the structure of the boundary layer induced by an inviscid flow of the form (2) is quite different from that originated by an inviscid flow like (4), they have in common that the non-existence of similarity solutions for r^{-1} -type flows over an infinite plane is not an isolated case.

The structure of the paper is as follows. Section 2 states the boundary-layer problem using several results from (14) concerning the structure of the external inviscid flow and the demonstration of the non-existence of self-similar solutions to the boundary-layer equations for the flow on an infinite solid plane, which are briefly summarized in two Appendices for convenience. In section 3, the boundary-layer equations are solved on a finite plane, a circular disk of radius R . It is shown there that, choosing the variables appropriately, the numerical solution tends to an asymptote, which depends only on a single similarity variable, as the axis is approached. In section 4, a similarity solution for the finite disk problem valid for $0 \leq r \leq R$ is given. This solution shows excellent agreement with the numerical results of the previous section. Finally, some conclusions are drawn in section 5.

2. Formulation of the problem

Since there is no self-similar solution for the boundary-layer problem induced by the inviscid flow (4) over an infinite solid plane (see Appendix B), we undertake here the numerical integration of

the boundary-layer equations. In cylindrical polar coordinates, assuming axisymmetry and that $\partial/\partial r \ll \partial/\partial z$, the equations that describe the flow may be written as

$$\frac{\partial(ru)}{\partial r} + \frac{\partial(rw)}{\partial z} = 0, \quad (6)$$

$$u \frac{\partial u}{\partial r} + w \frac{\partial u}{\partial z} - \frac{v^2}{r} = -\frac{\partial(p/\rho)}{\partial r} + \nu \frac{\partial^2 u}{\partial z^2}, \quad (7)$$

$$u \frac{\partial v}{\partial r} + w \frac{\partial v}{\partial z} + \frac{uv}{r} = \nu \frac{\partial^2 v}{\partial z^2}, \quad (8)$$

where ρ and ν are the fluid density and kinematic viscosity, and p is the pressure field, which is specified by the outer inviscid flow. These equations will be solved with a no-slip boundary condition at the plane wall,

$$u = v = w = 0 \quad \text{for } z = 0, \quad (9)$$

and by matching to the inviscid flow outside the boundary layer of the form (4) with $1 \leq m < 2$ (actually the formulation given below is valid for $0 < m < 2$, but we will consider only the range of interest $1 \leq m < 2$).

To solve the problem numerically, one considers a finite wall. Thus we assume that the wall is a disk of radius R centred at the vortex axis. It must be noted here that the requirement for a finite disk is not only to solve the problem numerically, but to allow for the non-existence of steady self-similar solutions for $R \rightarrow \infty$. Obviously, the introduction of the length scale R destroys self-similarity.

Both at $r = R$ for any z , and as $z \rightarrow \infty$ for any r , the flow is given by the inviscid solution near the plane, which from (14) may be written as (note the change from the spherical polar coordinates of (14) to the present cylindrical ones; see Appendix A)

$$\Psi = (KQ)^m (rz)^{m/2} \left(1 - \frac{1}{2mQ^2} \frac{z}{r} + O\left(\frac{z^2}{r^2}\right) \right), \quad (10)$$

$$v = \frac{(KQ)^m}{Q} z^{(m-1)/2} r^{(m-3)/2} \left(1 - \frac{m-1}{2m^2Q^2} \frac{z}{r} + O\left(\frac{z^2}{r^2}\right) \right), \quad (11)$$

where the constant K is related to the circulation, and Q is a non-dimensional constant which depends on the swirl parameter L and on m (see (A.12), (A.13)). In (10) we have used the stream function for the meridional motion, through which the velocity components u and w are given by

$$rw = \partial\Psi/\partial r, \quad ru = -\partial\Psi/\partial z, \quad (12)$$

and the continuity equation (6) is automatically satisfied. Finally, the pressure term in (7) is also given by the inviscid solution near the plane, which from Appendix A may be written as

$$\frac{p}{\rho} = (KQ)^{2m} r^{2(m-2)} \left[\Pi_0 - \frac{m}{2} \left(\frac{z}{r}\right)^m + O\left(\frac{z^{m+1}}{r^{m+1}}\right) \right], \quad (13)$$

where $\Pi_0(L, m)$ is an integration constant.

To non-dimensionalize the problem, we define a Reynolds number,

$$\text{Re} = \frac{(KQ)^m R^{m-1}}{\nu}, \tag{14}$$

which is assumed large. It should be noted that this Reynolds number is based on a characteristic meridional velocity and the radius of the disk, so that it may be supposed to be large independently of the intensity of the swirl, if any; that is, $\text{Re} \gg 1$ for any value of L (or Q). Comparing the convective and viscous terms in (7) and (8) by using (10), (11) and (14), one obtains the following order of magnitude for the boundary-layer thickness δ (except near the disk edge; see (25) below):

$$\frac{\delta}{R} \sim \frac{1}{\text{Re}^{2/(m+2)}} \ll 1. \tag{15}$$

As a first step we undertook the numerical integration of the problem using the self-similar variables $\bar{\eta}$, \bar{F} and \bar{G} (equations (B.1) to (B.3)), with the obvious addition of the new independent variable $\xi = r/R$ to account for the non-self-similar radial variation of the flow. Numerical results using these variables are reported, for $m = 1$, in (18). It is shown that, although a self-similar solution to the problem depending only on $\bar{\eta}$ does not exist, for a finite disk the problem has indeed a non-self-similar solution which depends on both $\bar{\eta}$ and ξ . But the most important consequence of these preliminary numerical results is that they provide scaling laws which suggest the use of another set of dependent and independent variables in terms of which the solution tends, as we shall see, to an asymptote as the axis is approached ($\xi \rightarrow 0$).

In fact, the numerical results in (18) suggest the use of the following dimensionless variables (instead of (B.1) to (B.3) and together with ξ):

$$\xi = \frac{r}{R}, \quad \eta = \text{Re}^{2/(m+2)} \xi \frac{z}{R}, \tag{16}$$

$$\Psi = \nu R \text{Re}^{2/(m+2)} F(\xi, \eta), \tag{17}$$

$$v = \frac{\nu}{r} \text{Re}^{3/(m+2)} G(\xi, \eta). \tag{18}$$

The meridional velocity components become, in terms of F ,

$$u = -\frac{\nu}{R} \text{Re}^{4/(m+2)} F_\eta, \quad w = \frac{\nu}{R \xi^2} \text{Re}^{2/(m+2)} (\xi F_\xi + \eta F_\eta), \tag{19}$$

where the subscripts mean partial differentiation with respect to the corresponding variable. Equations (7), (8) become

$$F_{\eta\eta\eta} + \xi^{-2} (F_\eta F_{\xi\eta} - F_\xi F_{\eta\eta}) = \xi^{-4} [\text{Re}^{-2/(m+2)} G^2 + 2(2-m)\Pi_0 \text{Re}^{2(m-2)/(m+2)} \xi^{2(m-1)}], \tag{20}$$

$$G_{\eta\eta} + \xi^{-2} (F_\eta G_\xi - G_\eta F_\xi) = 0. \tag{21}$$

In the formal limit $\text{Re} \rightarrow \infty$, consistent with the lowest-order boundary-layer approximation given here, one may drop the terms on the right-hand side of (20) (note that $0 < m < 2$), so that it becomes decoupled from (21):

$$F_{\eta\eta\eta} + \xi^{-2} (F_\eta F_{\xi\eta} - F_\xi F_{\eta\eta}) = 0. \tag{22}$$

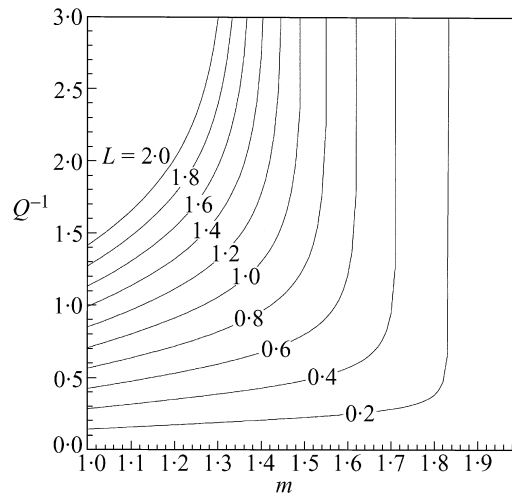


Fig. 1 Q^{-1} as a function of m for different values of L

The boundary condition (9) may be written as

$$F = F_\eta = G = 0 \quad \text{for} \quad \eta = 0, \quad 0 < \xi < 1. \quad (23)$$

The boundary conditions (10), (11) for $\eta \rightarrow \infty$, $0 < \xi < 1$, and $\xi = 1$, $0 < \eta < \infty$, become

$$F = \eta^{m/2} \left[1 - \frac{1}{2mQ^2} \frac{\eta}{\xi^2 \text{Re}^{2/(m+2)}} + \dots \right], \quad G = Q^{-1} \eta^{(m-1)/2} \left[1 - \frac{m-1}{2m^2 Q^2} \frac{\eta}{\xi^2 \text{Re}^{2/(m+2)}} + \dots \right]. \quad (24)$$

Terms proportional to negative powers of the Reynolds number are again neglected in the formal limit $\text{Re} \rightarrow \infty$, so that only the first terms above will be considered. Note from (A.12), (A.13) that $Q^{-1} \rightarrow \infty$ for $L = \sqrt{(2-m)/(m-1)}$, where the constant D in (A.12) becomes zero. Thus, for each m , no inviscid solution exists above this maximum value of L , and the present boundary-layer analysis ceases to be meaningful (this value of L is always larger than the critical swirl parameter for the breakdown of the vortex core; see (15)). The constant Q^{-1} is plotted in Fig. 1 as a function of m for several values of L .

An important feature of (21), (22) is that they do not depend on the parameters m and L . These inviscid parameters enter through the second boundary condition in (24). On the other hand, since equation (22) is decoupled from (21), the meridional motion (F) may be obtained independently of the azimuthal one (G). As a consequence, the meridional flow does not depend on the intensity of the swirl L (or Q), which affects only G through the second boundary condition in (24). This fact does not mean that the meridional and azimuthal motions are necessarily decoupled. Indeed, it is shown in (15) that only certain m -dependent ranges of values of L are allowed by the near-axis boundary layer that regularizes the inviscid flow (in particular, $L = \sqrt{2}$ is the only permissible value for $m = 1$ in *one-cell* flows; see (15 to 17)).

3. Numerical procedure and results

To integrate numerically the above equations, it is convenient to further transform the variables (the results will, however, be given in the variables (16) to (18)). First, one has to take into account that these variables are not appropriate near the edge of the disk because the boundary-layer thickness is zero there. The appropriate scaling factors near $\xi = 1$ are obtained from (7), (8) using (10), (11) with $r \sim R$:

$$\delta/R \sim [(1 - \xi)/\text{Re}]^{2/(m+2)}, \quad F \sim (1 - \xi)^{m/(m+2)}, \quad G \sim (1 - \xi)^{(m-1)/(m+2)}. \quad (25)$$

According to this, one defines the new independent and dependent variables for the numerical integration

$$\gamma = x^{-2/(m+2)}\eta, \quad x \equiv 3(1 - \xi), \quad (26)$$

$$f(\gamma, \xi) = x^{-m/(m+2)}F(\eta, \xi), \quad (27)$$

$$g(\gamma, \xi) = x^{(1-m)/(m+2)}G(\eta, \xi), \quad (28)$$

where the factor 3 in x has been added for later convenience. On the other hand, in order to improve the accuracy of the computations as the axis is approached, we redefine the radial coordinate as

$$l = -\ln \xi, \quad (29)$$

so that the interval $1 \geq \xi \geq 0$ is mapped onto $0 \leq l < \infty$. Substituting (26) to (29) into (21) to (24) one obtains

$$f_{\gamma\gamma\gamma} + \frac{3}{\xi^2} \left(\frac{m}{m+2} f f_{\gamma\gamma} + \frac{2-m}{m+2} f_{\gamma}^2 \right) + 3 \frac{1-\xi}{\xi^3} (f_{\gamma\gamma} f_l - f_{\gamma} f_{l\gamma}) = 0, \quad (30)$$

$$g_{\gamma\gamma} + \frac{3}{\xi^2} \left(\frac{1-m}{m+2} g f_{\gamma} + \frac{m}{m+2} f g_{\gamma} \right) + 3 \frac{1-\xi}{\xi^3} (g_{\gamma} f_l - f_{\gamma} g_l) = 0, \quad (31)$$

$$f = f_{\gamma} = g = 0 \quad \text{for} \quad \gamma = 0, \quad 0 < l < \infty, \quad (32)$$

$$f \rightarrow \gamma^{m/2}, \quad g \rightarrow Q^{-1} \gamma^{(m-1)/2} \quad \text{for} \quad \gamma \rightarrow \infty, \quad 0 < l < \infty \quad \text{and} \quad l = 0, \quad \gamma > 0. \quad (33)$$

To solve this problem numerically we use a finite difference method. Since the system (30), (31) is parabolic, one may start at the edge of the disk, $l = 0$, and proceed towards the axis, $l \rightarrow +\infty$, provided that the radial velocity remains negative ($f_{\gamma} > 0$), as will be the case in all the reported computations (see immediately below). To start the numerical computations, we use the solution in the formal limit $\xi \rightarrow 1$ ($l \rightarrow 0$). At the lowest order in $1 - \xi \ll 1$ ($l \ll 1$), f and g depend only on γ , and are given by the solution to the following set of two ordinary differential equations (the primes mean differentiation with respect to γ):

$$f''' + \frac{3m}{m+2} f f'' + \frac{3(2-m)}{m+2} f'^2 = 0, \quad (34)$$

$$g'' + \frac{3(1-m)}{m+2} g f' + \frac{3m}{m+2} f g' = 0, \quad (35)$$

with the boundary conditions

$$\gamma = 0, \quad f = f' = g = 0; \quad \gamma \rightarrow \infty, \quad f \rightarrow \gamma^{m/2}, \quad g \rightarrow Q^{-1}\gamma^{(m-1)/2}. \quad (36)$$

Since equations (34), (35) formally coincide with (B.6), (B.7) by just making $\gamma = \bar{\eta}$, $f = -\bar{F}$ and $g = \bar{G}$, one may use the general phase plane solution described there to obtain the starting condition for the numerical integration of (30), (31). It is worth mentioning here that the solution to (34) always yields a non-positive radial velocity (that is, $f_\gamma \geq 0$ for all γ) for every value m in the range under consideration. Thus, the starting radial velocity is always negative (zero at the plane), so that the flow (and the vorticity) is always convected towards the axis at the disk edge. Use of a marching procedure to start the numerical integration of (30) to (33) from the edge of the disk is therefore justified. This marching technique remains valid while the radial velocity remains non-positive, as is the case in all the results given below. In the notation of Phillips (19) the (singular) parabolic problem (30) to (33) is *type-0*, which permits marching techniques. This feature of the radial flow is in marked contrast to previous works without inviscid meridional flow, which involve both inward and outward flow for $m \neq 1$ (8). The absence of oscillatory behaviour in the radial velocity profile is obviously due to the outer inviscid inflow, which forces the inner viscous flow towards the axis. This forcing is absent in previous works, where the outer flow is purely circumferential, with the radial flow confined within the viscous boundary layer and vanishing at the edge.

One thus starts the numerical integration at a given $l_0 \ll 1$ using the solution to (34) to (36) as the initial solution (which contains errors $O(l_0)$). At each l -station, the nonlinear set of difference equations resulting from (30), (31) is solved iteratively until convergence is reached within a given tolerance. All the numerical computations given below have been obtained using $l_0 = 0.005$, radial and axial step sizes equal to $\Delta l = 0.025$ and $\Delta \gamma = 0.08$, respectively, and a truncation value of γ equal to $\gamma_\infty = 80$. The comparison of the numerical results given below with those obtained using smaller step sizes and l_0 , and larger γ_∞ , showed that the errors remained below 0.5 per cent in all the reported computations.

Figure 2 shows the non-dimensional stream function (F), negative radial velocity (F_η), and azimuthal velocity (G), as functions of η for decreasing values of ξ , as well as the non-dimensional radial and azimuthal shear stresses at the wall ($F_{\eta\eta}(\eta = 0, \xi)$ and $G_\eta(\eta = 0, \xi)$), for the case $m = 1$ with $L = \sqrt{2}$. (As mentioned in the Introduction, this is the only value of L allowed for $m = 1$ by the regularization of the inviscid flow at the axis, though other values of L are possible for a two-cell configuration of the inviscid flow.) Also shown in the figures are the near-plane inviscid solutions (24), which do not satisfy the boundary conditions at the plane (the inviscid F_η is singular at the plane). It must be noticed from (24) that, for $m = 1$, G approaches the constant Q^{-1} as $\eta \rightarrow \infty$, which is unity for $L = \sqrt{2}$ (see Fig. 1). Figure 3 shows the same functions, except for F , for $m = 1.4$ and $L = 0.5$.

The first thing one may remark from these results is that the numerical solution is not valid very near the axis (see Figs 2(d) and 3(c)). This is because the problem becomes singular at the axis as a consequence of the singularity of the external inviscid flow there (it should be noted that this failure has nothing to do with the marching procedure, since the radial velocity is always non-positive; see Figs 2(b) and 3(a)). This difficulty in the numerical integration as the centre of the disk is approached is found in all previous related works (5 to 8). As mentioned in the Introduction, this singular behaviour of the inviscid flow is regularized through a near-axis viscous core (analysed in (15)), obviously modified near the origin by its interaction with the present near-plane boundary layer. In any case, Figs 2(d) and 3(c) show that one can integrate the boundary-layer equations

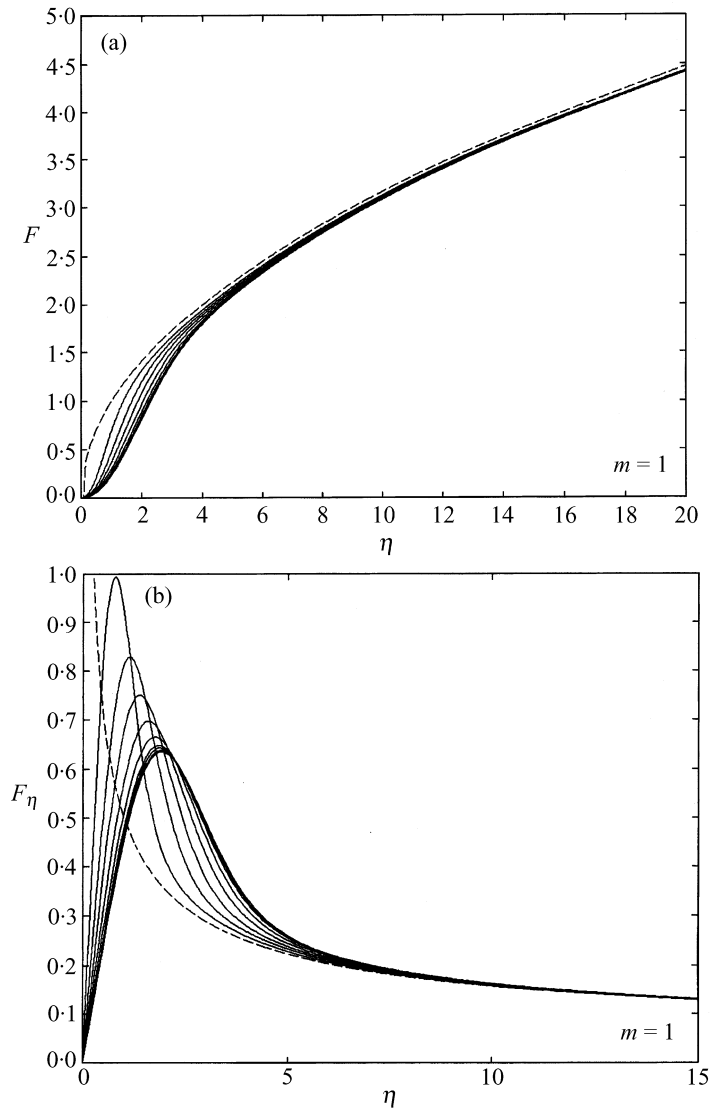


Fig. 2 (a) F , (b) F_η , and (c) G , vs. η for $\xi = 0.9, 0.8, \dots, 0.1$ with $m = 1$ and $L = \sqrt{2}$. The dashed lines correspond to the near-plane inviscid solutions (note that $Q^{-1} = 1$ for this case). (d) $F_{\eta\eta}(\eta = 0)$ and $G_\eta(\eta = 0)$ as functions of ξ for these values of m and L

numerically to reasonably low values of ξ (down to $\xi \simeq 0.05$, which is comparable to the numerical results for the interaction of a potential vortex with a plane of Prahlad and Head (6)), although whether the calculation remains physically meaningful at such low values of ξ can be determined only from the calculations of the full elliptical (Navier–Stokes) problem.

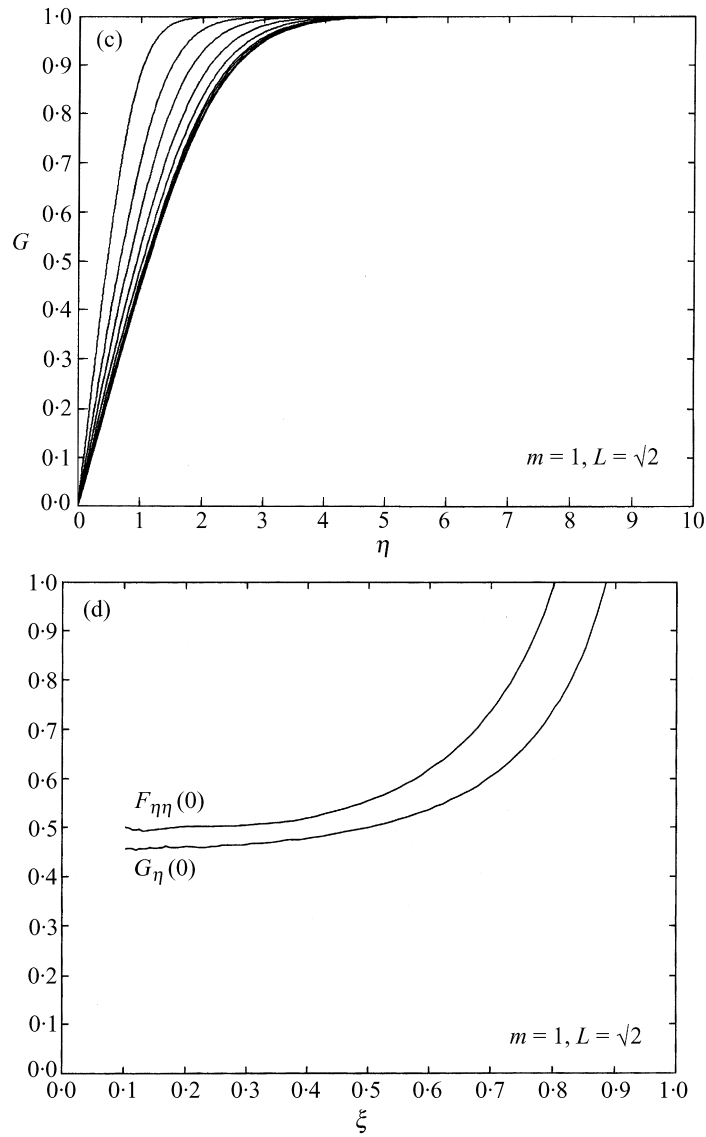


Fig. 2 cont.

4. Similarity solution for the finite disk problem

The above numerical results show the interesting feature that the solution approaches an asymptote, independent of the radial coordinate ξ , as $\xi \rightarrow 0$ (this is better appreciated in Figs 2(d) and 3(c)). Thus, as the axis is approached, the solution depends only on the similarity variable $\eta \sim rz$ in (16). This remarkable feature of the solution written in terms of the variables (16) to (18) is not shared by the solution in terms of the 'natural' self-similar variables of the problem ((B.1) to (B.3); see (18)).

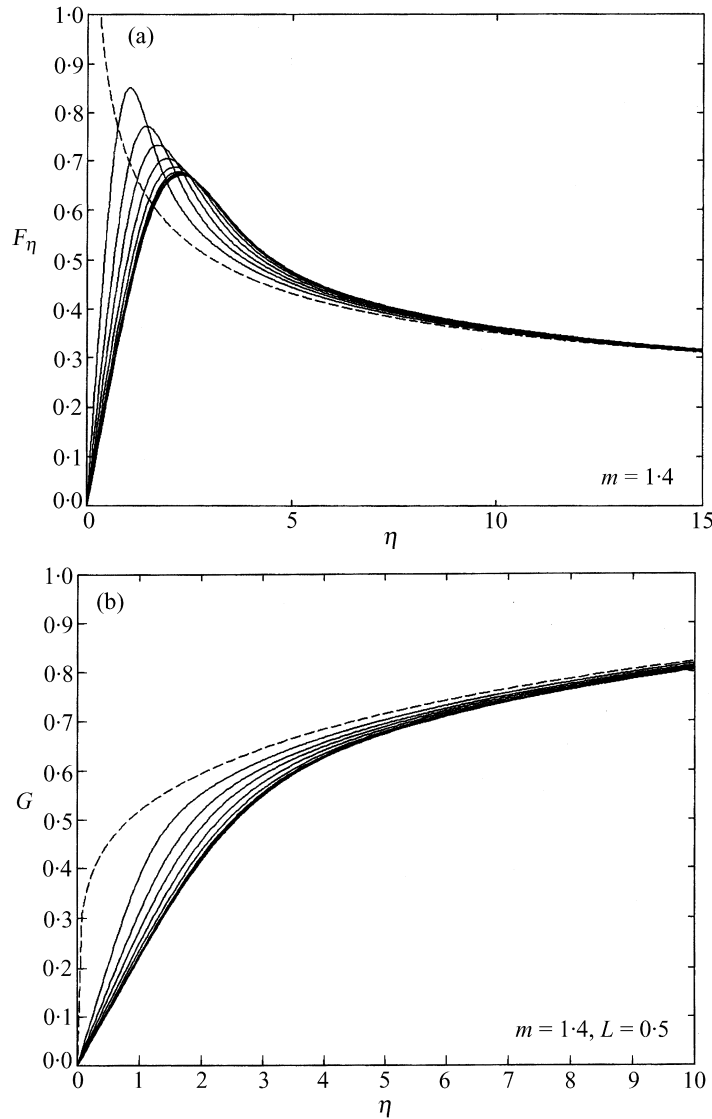


Fig. 3 (a) F_η , and (b) G , vs. η for $\xi = 0.9, 0.8, \dots, 0.1$ with $m = 1.4$ and $L = 0.5$. The dashed lines correspond to the near-plane inviscid solutions. (c) $F_{\eta\eta}(\eta = 0)$ and $G_\eta(\eta = 0)$ as functions of ξ

In both cases the boundary-layer equations depend explicitly on ξ , but only with (16) to (18) does the solution become independent of ξ as the axis is approached. This asymptotic solution valid far from the edge of the disk may be termed a self-similar solution of the *second kind* in the terminology of Barenblatt (20). In a previous version of this paper we obtained it by a small ξ expansion of the equations (actually, the expansion was in powers of ξ^3). However, Daniels (21) suggested that a

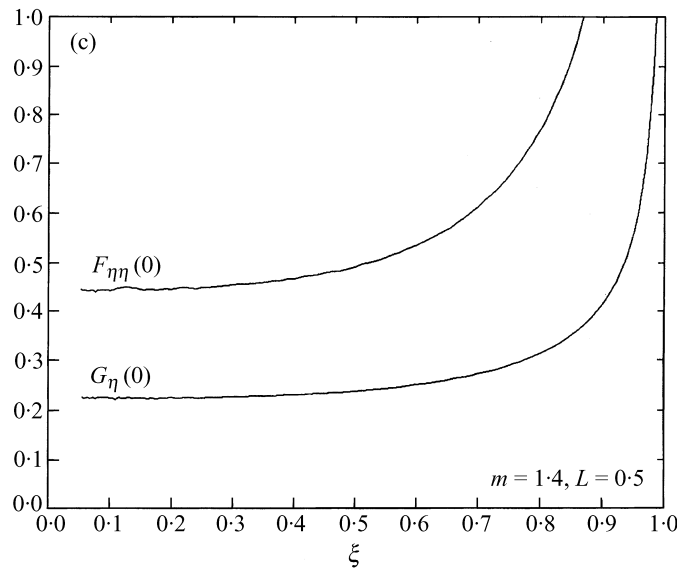


Fig. 3 cont.

similarity solution valid for all values of ξ might be found for the present finite disk problem. This solution is now given in this section.

In fact, if one uses the variables (26) to (28), but with

$$x = 1 - \xi^3 \tag{37}$$

instead of $x \sim 1 - \xi$, the independent variable ξ disappears from the problem. The new functions $f(\gamma)$ and $g(\gamma)$ satisfy (34) to (36) exactly for all values of ξ . As mentioned above, these equations coincide with (B.6) to (B.8) if one replaces $\overline{F}(\overline{\eta})$ by $-f(\gamma)$ and $\overline{G}(\overline{\eta})$ by $g(\gamma)$. The minus sign in \overline{F} is essential: Although (B.6) does not have a solution with negative radial velocity ($\overline{F}' > 0$) satisfying the boundary conditions (this being the reason why the present problem has no self-similar solution of the first kind, that is to say, a solution for an infinite plane), it does have a solution with $\overline{F}' < 0$ (see Appendix B), which, as we now see, provides a self-similar solution for the finite disk problem.

To integrate (34) numerically, one makes use of the two invariances enjoyed by this equation, reducing it to a first-order differential equation (see Appendix B). These invariances also allow the non-dimensional radial shear stress at the surface, $f''(0)$, to be obtained and therefore the complete solution, without the need of shooting. In terms of f , the radial velocity component is given by

$$u = -\frac{\nu}{R} \text{Re}^{4/(m+2)} (1 - \xi^3)^{(m-2)/(m+2)} f'(\gamma). \tag{38}$$

Figure 4 shows $f'(\gamma)$, for several values of m , and $f''(0)$ as m is varied. For $m = 1$, one easily obtains $f''(0) = \frac{1}{2}$ by just integrating (34) between 0 and ∞ . It must be remembered that f , and therefore the meridional motion, is independent of the swirl parameter L . In a similar way, the swirl

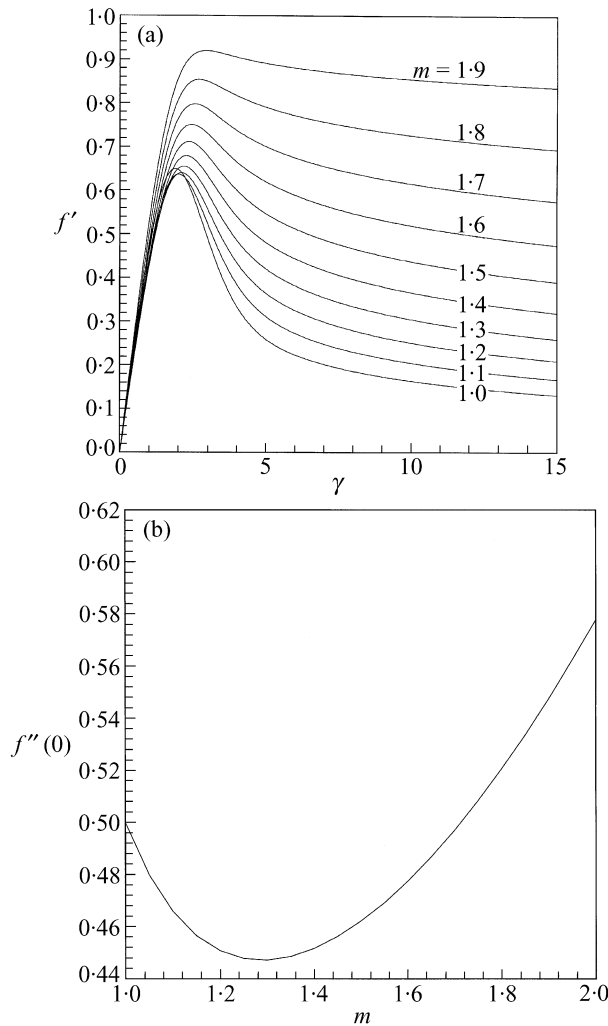


Fig. 4 (a) $f'(\gamma)$ for several values of m . (b) $f''(0)$ as m varies from 1 to 2

velocity is given by

$$v = \frac{v}{r} \text{Re}^{3/(m+2)} (1 - \xi^3)^{(m-1)/(m+2)} g(\gamma). \tag{39}$$

The only substantial difference from $f(\gamma)$ is that $g(\gamma)$ does depend on the swirl parameter L , as well as on m , through Q in (36). Figure 5 shows $g(\gamma)$ for several values of m and L , and $g'(0)$ as a function of m for different values of L . As in the case of $f''(0)$, $g'(0)$ is obtained without the need of shooting, but now by taking advantage of the linearity in g of (35).

The agreement between the present similarity solution and the numerical solution of the previous section is excellent. This can be seen in Fig. 6, where the non-dimensional radial and azimuthal shear stresses at the wall, $F_{\eta\eta}(0, \xi)$ and $G_{\eta}(0, \xi)$, obtained numerically, are compared with their

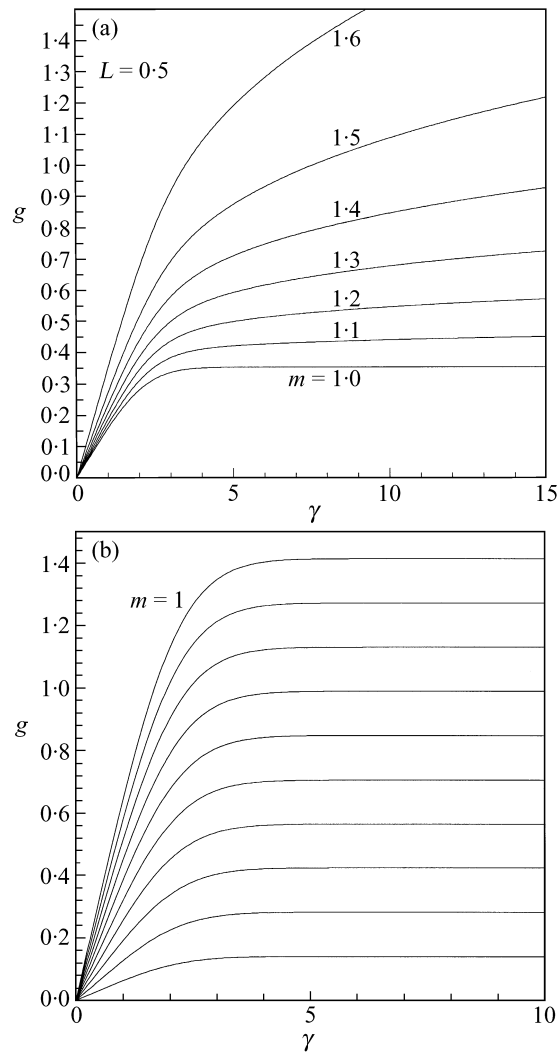


Fig. 5 (a) $g(\gamma)$ for several values of m with $L = 0.5$. (b) $g(\gamma)$ for $m = 1$ and various values of L (from bottom to top, $L = 0.2, 0.4, 0.6, 0.8, 1, 1.2, 1.4, 1.6, 2$). (c) $g'(0)$ as m varies from 1 to 2 for several values of L

self-similar counterparts, $(1 - \xi^3)^{(m-4)/(m+2)} f''(0)$ and $(1 - \xi^3)^{(m-3)/(m+2)} g'(0)$, respectively, for several values of m and L .

5. Conclusions

We have analysed in this paper the boundary-layer structure of the flow induced on a plane wall by the family of inviscid vortices with conical symmetry (4). In spite of the self-similar structure of the infinite plane problem, no solution exists, as was already known for a particular member of the family of inviscid vortices ($m = 1$; see for example, (10) to (13)), and as was shown in general

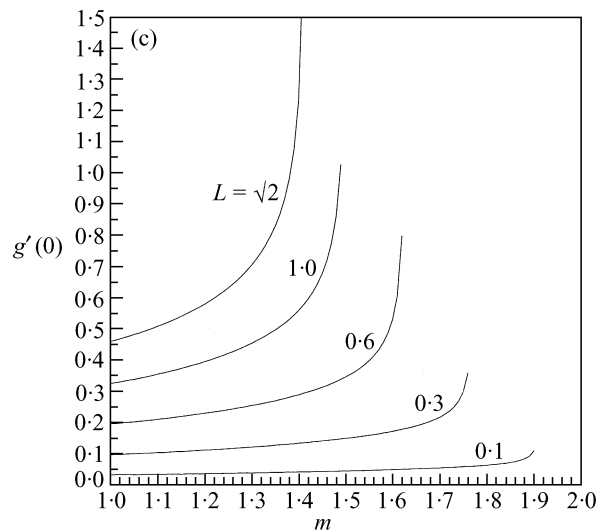


Fig. 5 cont.

(for $0 < m < 2$) in (14) (see Appendix B). The particular case with $m = 1$ has often been used as an idealized model for tornadoes, and other atmospheric and technological vortices (10) to (12). The generalization to values of $m \neq 1$, particularly for $1 < m < 2$, is of interest because several swirling flows of technological and atmospheric significance at high Reynolds numbers behave like (4) outside the viscous vortex core, with m slightly larger than unity (9, 15, 22).

We have solved the boundary-layer equations numerically on a circular disk of radius R perpendicular to the axis of the vortex. We have found that a solution actually exists for the finite plane problem. This solution tends to an asymptote as the axis is approached that depends only on $\eta \sim rz$, being independent of the other variable, $\xi = r/R$, as $\xi \rightarrow 0$. It is found numerically that this asymptote is in fact approximately valid for relatively large values of ξ . More remarkable is the fact that the finite disk problem has a self-similar solution that depends only on the similarity variable

$$\gamma \sim \frac{rz}{[1 - \xi^3]^{2/(m+2)}} \tag{40}$$

The ordinary differential equations governing the finite disk self-similar problem are formally the same as those that govern the infinite plane one, but with the essential difference that now there exists a trajectory on the phase plane connecting the boundary conditions, which for the infinite plane problem did not exist. Thus, the introduction of a new characteristic length, the radius of the disk R , which destroys the self-similarity of the infinite plane problem, surprisingly allows for a self-similar solution. Nonetheless, the finite radius of the disk R remains essential in this solution, no matter how small is ξ (see, for instance, (38)). Due to the nature of the inviscid external flow, the structure of this similarity solution is simpler than other (two-layer) similarity solutions of related boundary-layer flows over a finite disk (5, 7, 8).

As a final remark it must be pointed out that, although our numerical calculations in section 3 are valid even for very small distances to the centre of the disk (as low as $\xi \simeq 0.05$), they obviously fail before the axis is reached, where the inviscid external flow considered becomes

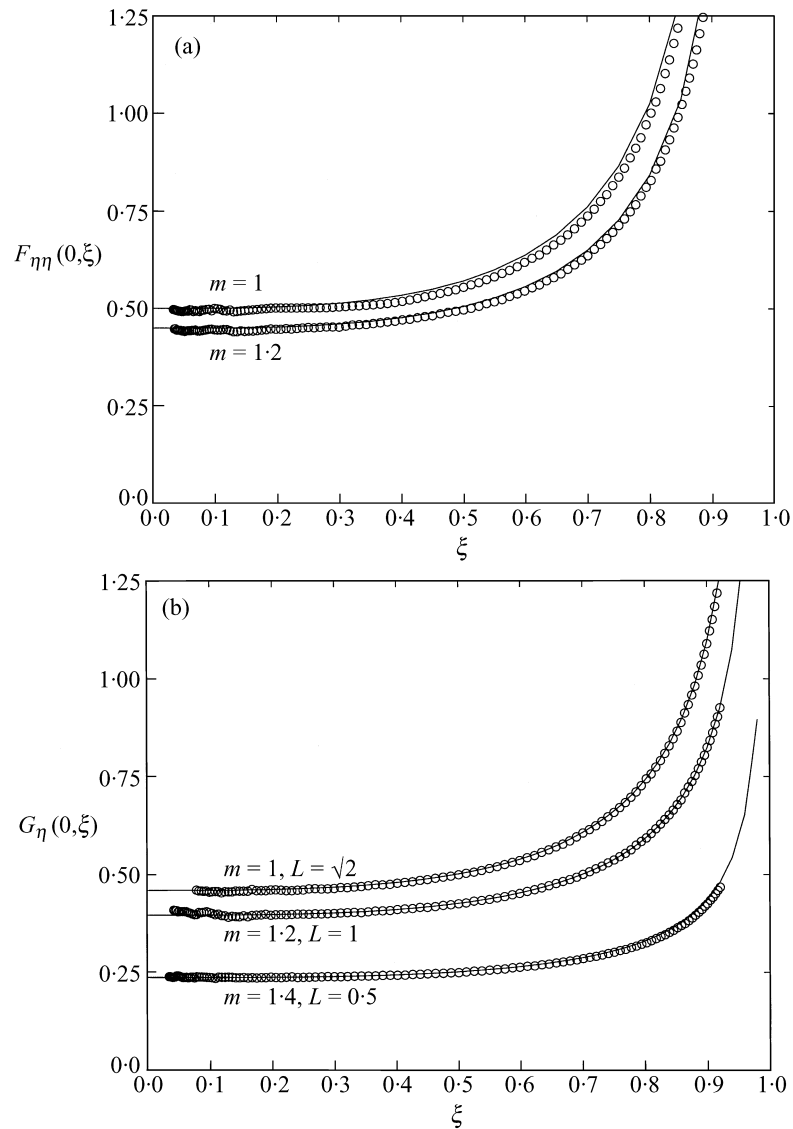


Fig. 6 (a) $F_{\eta\eta}(0, \xi)$ obtained numerically (circles) compared to the similarity solution, $(1 - \xi^3)^{(m-4)/(m+2)} f''(0)$, for $m = 1$ and $m = 1.2$. (b) $G_{\eta}(0, \xi)$ obtained numerically (circles) compared to the similarity solution, $(1 - \xi^3)^{(m-3)/(m+2)} g'(0)$, for several values of m and L

singular. Actually, the radial inward flow inside the boundary layer turns upward near the axis to form the rising viscous core of the vortex (22 to 23), which regularizes the inviscid flow at the axis (15). The self-similar solution given here provides, for $\xi \rightarrow 0$, very simple and useful initial velocity profiles to consistently model the effusing core structure in some flows of geophysical technological interest. Obviously, this effusing core flow cannot be modelled by a boundary-layer

approximation. One has to solve the full incompressible Navier–Stokes equations numerically (the problem also becomes Reynolds-number dependent) using the similarity solution near the axis as the inlet boundary condition, a task which is beyond the objective and scope of the present paper.

Acknowledgements

Comments by a referee led to the improvement of an earlier version of section 4. The similarity solution given in that section is due to Professor P. G. Daniels, to whom we are indebted. This work has been supported by the DGES of Spain grant PB96-0679-C02-01. A NATO Collaborative Research grant, CRG 950368, is also acknowledged.

References

1. G. I. Taylor, *Q. Jl Mech. appl. Math.* **3** (1950) 129–139.
2. N. Rott and W. S. Lewellen, In *Progress in Aeronautical Sciences* (ed. D. Kuchemann; Pergamon, Oxford 1966).
3. W. S. King and W. S. Lewellen, *Phys. Fluids* **7** (1964) 1674.
4. U. T. Bödewadt, *ZAMM*, **20** (1940) 241.
5. O. R. Burggraf, K. Stewartson and R. J. Belcher, *Phys. Fluids* **14** (1971) 1821–33.
6. T. S. Prahlad and M. R. Head, *Computers and Fluids*, **4** (1976) 157–169.
7. G. F. Carrier, F. E. Fendell and P. S. Feldman, *Proceedings of the 15th Conference on Severe Local Storms* (Amer. Meteor. Soc., Boston, MA 1988) 331–334.
8. R. J. Belcher, O. R. Burggraf and K. Stewartson, *J. Fluid Mech.* **52** (1972) 753–780.
9. A. Ogawa, *Vortex Flows* (CRC Press, London 1993).
10. C. Sozou, *J. Fluid Mech.* **244** (1992) 633–644.
11. J. Serrin, *Phil. Trans R. Soc. A* **271** (1972) 327–360.
12. V. Shtern and F. Hussain, *Phys. Fluids A* **5** (1993) 2183–2195.
13. M. A. Goldshtik, *Appl. Mat. Mech. (Sov.)* **24** (1960) 610–621.
14. R. Fernandez-Feria, J. Fernandez de la Mora, M. Perez-Saborid and A. Barrero, *Q. Jl Mech. appl. Math.* **52** (1999) 1–53.
15. —, — and A. Barrero, *J. Fluid Mech.* **305** (1995) 77–91.
16. R. L. Long, *ibid.* **11** (1961) 611–625.
17. M. A. Goldshtik and V. M. Shtern, *ibid.* **218** (1990) 483–508.
18. J. C. Arrese and R. Fernandez-Feria, *Proc. 4th Ann. Conf. of the CFD Soc. of Canada* (Ottawa 1996) 697–704.
19. W. R. C. Phillips, *J. Fluid Mech.* **319** (1996) 151–170.
20. G. I. Barenblatt, *Scaling, Self-Similarity, and Intermediate Asymptotics* (Cambridge University Press, Cambridge 1996).
21. P. G. Daniels, private communication.
22. M. R. Head, T. S. Prahlad and W. R. C. Phillips, *Aeronautical Q.* **28** (1977) 197–22210.
23. W. R. C. Phillips, *Phys. Fluids* **27** (1984) 2215–2220.

APPENDIX A

Inviscid outer flow

In this Appendix we summarize from (14) the solutions to the steady Euler equations for an incompressible fluid

$$\nabla \cdot \mathbf{u} = 0, \quad \rho \mathbf{u} \cdot \nabla \mathbf{u} + \nabla p = 0, \quad (\text{A.1})$$

of the form

$$\Psi = \Phi(y)r^m, \quad y \equiv r/z, \quad (\text{A.2})$$

$$v = \Omega(y)r^{m-2}, \quad \frac{p}{\rho} = \Pi(y)r^{2(m-2)}. \quad (\text{A.3})$$

Substituting these expressions into (A.1), one obtains the following three ordinary differential equations for Φ , Ω and Π :

$$(m-2)y^4\Phi'^2 - 2my^3\Phi\Phi' - my^4\Phi\Phi'' - \Omega^2 + 2(m-2)\Pi + y\Pi' = 0, \quad (\text{A.4})$$

$$(m-1)\Phi'\Omega = m\Phi\Omega', \quad (\text{A.5})$$

$$\Pi' = (m-2)y\Phi'^2 - 3m\Phi\Phi' - my\Phi\Phi''. \quad (\text{A.6})$$

As shown in (14), this system can be integrated twice, and is thus reduced to the integration of just one ordinary differential equation for Φ (note that in (14) spherical polar coordinates are used instead of the cylindrical ones used here):

$$y^2(1+y^2)\Phi'' + y(2m-1+2y^2)\Phi' + m(m-2)\Phi = K_1 \frac{2(m-2)}{m} \Phi^{1-4/m} - K^2 \frac{m-1}{m} \Phi^{1-2/m}, \quad (\text{A.7})$$

where Ω and Π are given as functions of Φ as

$$\Omega = K\Phi^{(m-1)/m}, \quad (\text{A.8})$$

$$\Pi = K_1\Phi^{2-4/m} - \frac{1}{2}(m\Phi + y\Phi')^2 - \frac{1}{2}y^4\Phi'^2 - \frac{1}{2}\Omega^2, \quad (\text{A.9})$$

and K and K_1 (≥ 0) are arbitrary constants related to the intensities of the swirl and the meridional motion, respectively (more precisely, K and K_1 are related to Kelvin and Bernoulli theorems, respectively; see (14)). In non-dimensional form, defining

$$Y \equiv \frac{\Phi}{K^m}, \quad D \equiv \frac{2(2-m)K_1}{mK^4}, \quad (\text{A.10})$$

where $D > 0$ for $m < 2$, one has

$$y^2(1+y^2)Y'' + y(2m-1+2y^2)Y' + m(m-2)Y + DY^{1-4/m} + \frac{m-1}{m}Y^{1-2/m} = 0. \quad (\text{A.11})$$

Near the axis the solution is singular, but it can be regularized through a viscous core with self-similar structure. It is shown in (15) that, for $0 < m < 2$, the regularization is possible only for certain ranges of the swirl parameter (5), which is related to D through (see (14))

$$D = \frac{2-m-(m-1)L^2}{m^3L^4}. \quad (\text{A.12})$$

It is also shown in (15) that only those inviscid flows with upward axial velocity ($\Phi' \geq 0$) can be regularized at the axis.

We are interested here in the behaviour of the solutions of (A.11) near a plane wall perpendicular to the axis of the vortex. Making $Y \rightarrow 0$ for $y \rightarrow \infty$ in (A.11), one obtains

$$Y \sim Q^m y^{-m/2} \left(1 - \frac{1}{2mQ^2 y} + O(y^{-2}) \right), \quad Q = \left(\frac{4D}{m(2-m)} \right)^{1/4}. \quad (\text{A.13})$$

It should be noted that the behaviour of the solution near any conical wall coaxial with the vortex is very similar to (A.13) if one uses spherical polar coordinates. Therefore, the analysis given in this work for the boundary layer near a plane wall can easily be extended to the boundary layer on a conical wall. In fact, the dimensionless boundary-layer equations given below are exactly the same.

APPENDIX B

Non-existence of a self-similar solution of the first kind

Next we summarize, also from (14), the demonstration that no self-similar solution to the problem for an infinite plane (6) to (11) exists. The formal comparison of convective and viscous terms in (7), (8), using (10), (11) when no characteristic length is present, yields the radial dependence of the boundary-layer thickness δ , of Ψ , and of v , for a self-similar boundary layer:

$$\bar{\eta} = \frac{z}{\delta(r)}, \quad \delta(r) = \left[\frac{v}{(KQ)^m r^{m-1}} \right]^{2/(m+2)} r, \quad (\text{B.1})$$

$$\Psi = \frac{vr^2}{\delta(r)} \bar{F}(\bar{\eta}) = vRRe^{2/(m+2)} \xi^{3m/(m+2)} \bar{F}(\bar{\eta}), \quad (\text{B.2})$$

$$v = \frac{vr^{1/2}}{\delta(r)^{3/2}} \bar{G}(\bar{\eta}) = \frac{v}{R} Re^{3/(m+2)} \xi^{(2m-5)/(2+m)} \bar{G}(\bar{\eta}), \quad (\text{B.3})$$

which, in the case that F and G are independent of ξ , are related to the variables in (16) to (18) through

$$\eta = \xi^{6/(m+2)} \bar{\eta}, \quad F = \xi^{3m/(m+2)} \bar{F}, \quad G = \xi^{3(m-1)/(m+2)} \bar{G}. \quad (\text{B.4})$$

The meridional velocity components may be written as

$$u = -\frac{vr}{\delta(r)^2} \bar{F}', \quad w = \frac{v}{(m+2)\delta(r)} [3m\bar{F} - (4-m)\bar{\eta}\bar{F}'], \quad (\text{B.5})$$

where the primes mean differentiation with respect to $\bar{\eta}$. Equations (7), (8) become

$$\bar{F}''' + \frac{3(m-2)}{m+2} \bar{F}'^2 - \frac{3m}{m+2} \bar{F}\bar{F}'' = 0, \quad (\text{B.6})$$

$$\bar{G}'' + \frac{3(m-1)}{m+2} \bar{F}'\bar{G} - \frac{3m}{m+2} \bar{F}\bar{G}' = 0, \quad (\text{B.7})$$

where, again, the radial momentum equation (B.6) is decoupled from the azimuthal one (B.7). One is interested in the solution to these equations satisfying the boundary conditions

$$\bar{\eta} = 0, \quad \bar{F} = \bar{F}' = \bar{G} = 0; \quad \bar{\eta} \rightarrow \infty, \quad \bar{F} \rightarrow \bar{\eta}^{m/2}, \quad \bar{G} \rightarrow Q^{-1}\bar{\eta}^{(m-1)/2}. \quad (\text{B.8})$$

Equation (B.6) may be reduced to a first-order differential equation by making use of its invariance under two uniparametric groups of transformations, suggesting the new variables

$$q = \frac{\bar{F}'}{\bar{F}^2}, \quad t = \bar{F} \frac{dq}{d\bar{F}}, \quad (\text{B.9})$$

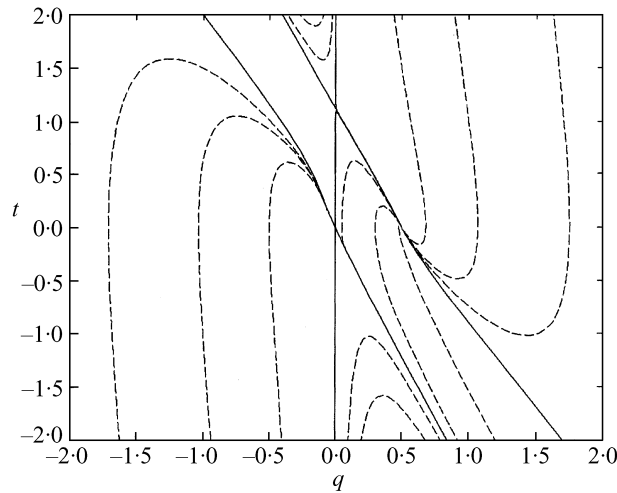


Fig. 7 (t, q) -phase plane for $m = 1.2$

through which (B.6) becomes

$$\frac{dt}{dq} = \frac{-7tq + 3q - 6q^2 - t^2 + \frac{3m}{m+2}t}{tq}. \quad (\text{B.10})$$

An exhaustive phase plane analysis of this equation is given in (14). As a representative case in the range $1 < m < 2$, we show in Fig. 7 the phase plane corresponding to $m = 1.2$. Since the radial velocity has to be negative ($\bar{F}' \geq 0$), the solution which one is looking for must correspond to a trajectory lying in the quadrant ($q \geq 0, t \leq 0$). It must behave as $t = -3q/2$ as both $t, q \rightarrow \infty$, which corresponds to zero velocity at the plane, and go to the origin ($q = 0, t = 0$) as $t = -(m+2)q/m$, corresponding to the inviscid behaviour. However, no trajectory in the phase plane of Fig. 7 shows this behaviour: the distinguished trajectory starting at infinity as $t = -3q/2$ goes to the singular point ($q = 0, t = \frac{1}{2}$), which yields a singular behaviour for $\bar{F}(\bar{\eta})$ with no physical meaning. On the other hand, the trajectory coming from the origin with the above mentioned behaviour, dies at infinity as $t = -2q$, which is incompatible with a no-slip boundary condition at the plane. Therefore, no solution to (B.6) satisfying the boundary conditions (B.8) exists for the case $\bar{F}' \geq 0$. It should be noticed, however, in Fig. 7 that a trajectory satisfying both boundary conditions exists in the quadrant ($q \leq 0, t \geq 0$). But this solution corresponds to a positive radial velocity at the plane and, therefore, to an inviscid flow going downwards at the axis, which cannot be regularized through a near-axis viscous core (see (15); the flow configuration considered here, consisting of a near-plane flow towards the axis, going upward at the axis, is, on the other hand, that observed in real vortices such as tornadoes). Nonetheless, that trajectory plays an important role in the similarity solution for the finite disk problem given in section 4.